The characteristics of ambient seismic noise as a source for surface wave tomography

Yingjie Yang and Michael H. Ritzwoller

Center for Imaging the Earth's Interior

Department of Physics

University of Colorado at Boulder

Boulder, CO 80309-0390

303-735-1850

yingjie.yang@colorado.edu

Abstract

Inter-station cross-correlations of ambient seismic noise from one year of continuous data at periods between 6 and 100 sec are used to study the origin of the ambient noise using stations located in Europe, southern Africa, Asia, and three regions within North America. The signal-to-noise ratios (SNR) of Rayleigh waves for positive and negative correlation time lags at periods of 8, 14, 25 and 50 sec provide the azimuthal distribution of strong ambient noise sources. Ambient noise in both the primary (10-20 sec) and secondary microseism bands (5-10 sec) comes dominantly from the directions of relatively nearby coastlines with stronger noise occurring in the northern hemisphere in northern winter and in the southern hemisphere in southern winter, consistent with the hypothesis that oceanic microseisms are generating this noise. The observed differences in the directivity of noise in the primary and secondary microseism bands are the consequence of propagation and attenuation, rather than the generation mechanism. At intermediate and long periods (> 20 sec), there is much less seasonal variation in both signal strength and directivity. Our results are explained most simply by near-coastal sources rather than deep ocean sources at all periods. Although the dominant ambient noise sources are distributed inhomogeneously in azimuth, strong ambient noise emerges from most directions when using recordings that are one-year in duration. This is what ensures the accuracy of the empirical Green's functions and ambient noise tomography.

1. Introduction

Cross-correlations of random wavefields have been shown to recover empirical Green's functions between two receivers in a number of disciplines. In seismology, two types of signals have been considered to form random wavefields. The first is seismic coda, which results from the multiple scattering of seismic waves by small-scale inhomogeneities [e.g., *Aki and Chouet*, 1975; *Paul et al.*, 2005]. The second is ambient seismic noise. Ambient noise, in contrast with seismic coda, has the advantage that it

does not depend on earthquake occurrence and can be recorded at any time and any location.

Recently, surface wave tomography for Rayleigh waves based on cross-correlations of ambient seismic noise has been applied successfully to real data at regional scales, such as in the western US [*Shapiro et al*., 2005; *Sabra et al.*, 2005; *Moschetti et al.*, 2007; *Lin et al.*, 2007b], South Korea [*Cho et al.*, 2006], Tibet [*Yao et al.*, 2006], New Zealand [*Lin et al.*, 2007a], Iceland [*Gudmundsson et al.*, 2007], and southern Africa [*Yang et al.*, 2007b], and at continental scales, such as in Europe [*Yang et al.*, 2007a] and North America [*Bensen et al.*, 2007b]. The basic assumption underlying ambient noise tomography is that ambient seismic noise can be considered to be composed of random wavefields when taken over sufficiently long times, such as a year. A perfectly random distribution of the sources of ambient noise would result in symmetric cross-correlations with energy arriving at both positive and negative correlation lag times, usually referred to as the causal and acausal arrivals. In practice, however, significant asymmetry of the cross-correlations is often observed, which results from stronger or closer ambient noise sources directed radially away from one station than the other. Although *Derode et al.*, [2003] showed experimentally that inhomogeneous source distributions have lesser effects on the travel times of the waves than on their signal-to-noise ratios, such source distributions may interfere at some level with the ability to obtain reliable Green's functions and measure dispersion curves on them. A better understanding of the origin of ambient noise sources and their temporal and spatial distribution is needed, therefore, to ensure that ambient noise tomography is being developed on a firm footing.

Ambient seismic noise in the short period band (< 20 s), commonly referred to as microseisms, is related to the interaction of ocean swells with the seafloor near coastlines. Two strong peaks of the short-period seismic noise are typically observed in the primary (10-20 sec) and secondary (5-10 sec) microseism bands. The exact generation mechanism of the microseisms is not completely understood, but it is commonly believed that the

primary microseism involves direct interaction of ocean swells with the shallow seafloor [*Hasselmann,* 1963]. It is believed that the secondary microseism, with double-frequency signals relative to the primary microseism, is generated by the nonlinear interaction between the direct wave and coastline-reflected waves [*Longuet-Higgins,* 1950]. Long-period seismic noise, referred to as earth "hum", is observed in the continuous background free oscillations in low-frequency seismic spectra [*Nawa et al.,* 1998]. This term is usually reserved for motions with periods above 100 sec. Early studies attributed the long-period noise to atmospheric motions [*Tanimoto and Um,* 1999; *Ekstrom,* 2001], but more recent studies [*Tanimoto,* 2005; *Rhie and Romanowicz,* 2004; *Rhie and Romanowicz,* 2006], suggest that the origin of the long-period noise is more likely related to so-called ocean infragravity waves, a long-period ocean gravity wave. *Rhie and Romanowicz* [2004] proposed that the generation of long-period seismic noise involves a three stage atmosphere-ocean-seafloor coupling process.

The procedure to use long-duration cross-correlations to study the long-range correlation properties of ambient seismic noise was developed by *Stehly et al.* [2006]. They applied the method to about 20 stations in each of California, the eastern US, Europe, and Tanzania and found that ambient noise in the secondary microseism band is seasonally stable and emerges predominantly from nearby coastlines. In contrast, the primary microseism and longer period ambient noise (below 40 sec period) vary seasonally in similar ways and emerge from directions that may not be toward the local coasts. This observation appeared to them to sever the hypothesized physical link between the primary and secondary microseisms, and called into question the commonly believed casual relation between these waves. These authors argue that the cause of the primary microseism and the longer period ambient noise is ocean wave activity in deep water. This conclusion is at variance with the study of *Rhie and Romanowicz* [2006], which is based on detailed observations performed on seismic arrays in Japan and California during a large storm in the Pacific. *Rhie and Romanowicz* conclude that at all

periods, from the secondary microseism at several seconds period to earth hum at 240 sec, ocean wave energy is coupled to the solid earth predominantly near coastlines. They argue that nonlinear ocean wave-wave interactions near the coast generate long period energy, which propagates globally both as seismic waves in the solid earth and infragravity waves in the ocean which can then liberate their energy to the solid earth later, elsewhere. This mechanism may imply that ambient noise is not uniformly distributed in time or space, which may vitiate assumptions that underlie ambient noise tomography, however.

In this study, we follow the methodology of *Stehly et al.* [2006], but apply the method to a much larger station set in Europe, southern Africa, Tibet, and North America using 12 months of ambient noise data over a broad period band from 6 to 100 sec, which covers the microseism band as well as longer period noise. By analyzing the strength and quality of the cross-correlations in different seasons, directions, and period bands, we address three principal questions. First, we consider whether the primary and secondary microseisms behave differently and, hence, may be physically decoupled. Second, we ask whether the observations are consistent with generation in shallow coastal waters at all periods require a deep-water source at long-periods. Finally, we consider whether the resulting azimuthal distribution of ambient seismic noise is sufficiently homogeneous when taken over long times for ambient noise tomography to be successful. We focus on Rayleigh waves, so the results for Love waves may differ. We proceed by first looking at results from Europe, and then bring in results using arrays in southern Africa, Tibet, and North America.

Throughout the paper, we will refer to the “source” of ambient noise, and our use of this term requires clarification. By “source location”, we refer to the place or places where seismic waves within the solid earth are generated. The proximate cause of the seismic waves may be the interaction of gravity waves in the ocean with the seafloor. Identification of the ultimate cause of ambient noise involves a regress of physical

mechanisms that may have involved the generation of ocean gravity waves, the generation of large ocean storms from the interaction of winds with the ocean surface, storm formation in the atmosphere, differential solar forcing, and so on. Seismic waves, however, are blind to all processes that occurred prior to their generation, although the location of their formation, their frequency content, seasonal variability, and radiation pattern may provide clues about earlier processes. Thus, by the "source", "source location", and "cause", we will refer only to that place where and mechanism by which the seismic waves are generated.

Finally, it is important to acknowledge at the outset that the method of source characterization that we use is ambiguous and the arguments presented herein are qualitative in nature. The method only is capable of determining the relative direction to the principle source locations observed at an array, and inferences drawn about absolute locations must be made on the basis of plausibility and simplicity.

2. Initial analysis: Cross-correlations of ambient noise in Europe

We use continuous vertical-component seismic data from ~125 stations from the Global Seismic Network (GSN) and the Virtual European Broad-Band Seismic Network (VEBSN) (Figure 1) over the 12 months of 2004. The data processing procedure applied here is similar to that described at length by *Bensen et al.* [2007a]. Raw seismic data are processed one day at a time for each station after being decimated to 1 sample per second, and are band-pass filtered in the period band from 5 to 100 sec after the daily trend, the mean and the instrument response are removed. Filtered daily data are then normalized in time and whitened in this frequency band to remove earthquake signals and instrumental irregularities prior to performing cross-correlation. Daily cross-correlations are computed between all station-pairs and are then added to one another or stacked to produce two five-month and one one-year time series. The two five-month stacks are centered on January and July respectively; namely, months 11, 12, 1, 2, 3 and months 5, 6, 7, 8, 9.

The five-month stacks are used to investigate the seasonal variability of the ambient noise source.

Examples of 12-month cross-correlations are plotted in Figure 2 with the corresponding path segments shown in the bottom map. For each cross-correlation, surface wave signals coming from the two opposite directions between the stations appear at positive (casual component) and negative (acausal component) correlation time lag, respectively. The incoming directions of seismic noise contributing to the positive components are marked with arrows showing the directions of propagation along each path segment in Figure 2f. The positive components are for waves coming mostly from the northerly direction. The amplitude of the causal and acausal components depends on the strength and density of sources of ambient noise in line with the stations. Although signals coming from opposite directions sample the same structure between a station pair, the source characteristics, such as distance, strength, duration, frequency content and so on, may be very different on the two opposite sides. Thus, the resulting cross-correlations are often asymmetric, as illustrated in Figure 2, and these properties may be period dependent. For example, the higher amplitude arrivals in Figure 2 are generally from the north; i.e., at positive lag. The negative lag components for station-pairs ECH-TUE and DSB-TUE are nearly flat, indicating that there is relatively little energy arriving from the southeast. There is, however, substantial energy at negative lags for the pairs GRFO-TUE, MORC-TUE and KWP-TUE, resulting from waves coming from the southwest. There is also apparently a difference in frequency content at positive and negative lags. The best example is probably MORC-TUE, where a clear low frequency precursor appears at positive lag (coming from the northeast), which is missing at negative lag.

To demonstrate the frequency content of the signals in Figure 2, we plot in Figure 3 normalized amplitude spectra of the positive (right) and negative (left) lag components of the corresponding cross-correlation time-series. In each case, 1000-second time series are used to compute the spectrum, starting from zero lag. The lower curve in each panel is

the normalized spectrum of trailing noise contained in the 1000 sec time window starting at ±1000 sec lag time, which is always well removed from the surface wave signals. To illustrate the frequency-dependent characteristics of ambient noise sources, we divide the entire frequency band into three sub-bands: namely, low frequency noise LFN (0-0.05 Hz), the primary microseism band MS1 (0.05-0.1 Hz), and the secondary microseism band MS2 (0.1-0.2 Hz). For cross-correlations between the station pairs GRFO-TUE, MORC-TUE and KWP-TUE, there are strong low frequency noise signals on the positive components (Fig. 2b,c,d; and Fig. 3d,f,h), which come from the northeast quadrant (Fig. 2f). For the cross-correlations ECH-TUE and DSB-TUE, strong microseismic noise signals are observed on the positive components (Fig. 2a,e; and Fig. 3b,j), coming from the northwest quadrant, but little energy is observed in the low frequency band. The lack of high-frequency noise from a particular direction probably is a consequence of a distant source. The frequency-dependent characteristics of noise signals in strength and incoming direction are discussed in more detail in the next section for Europe and then in subsequent sections for elsewhere in the world.

To evaluate the quality and amplitude of the cross-correlations quantitatively, we calculate the period-dependent signal-to-noise (SNR) for the positive and negative components of each cross-correlation. SNR is defined as the ratio of the peak amplitude within a time window containing the surface wave signals to the root-mean-square of the noise trailing the signal arrival window. The signal window is determined using the arrival times of Rayleigh waves at the minimum and maximum periods of the chosen period band (6 to 100 sec) using the global 3-D shear velocity model of Shapiro and Ritzwoller (2002). Period dependence of SNR is determined by applying a series of narrow band-pass (ranging form 5 to 10 mHZ) filters centered on a grid periods from 6 to 100 sec. Figure 4a shows an example of a positive component broadband cross-correlation (bottom panel) along with seven narrow band-pass filtered time series. Rayleigh wave signals show up clearly in each of these bands. Figure 4b displays the

corresponding SNR as a function of period. SNR in this example (and generally) peaks in the primary microseism band (10-20 sec), around 14 sec period.

3. Sources of ambient noise observed in Europe

To investigate the directions of the incoming ambient noise systematically, we plot in Figure 5 the azimuthal distribution of SNR for the positive and negative components of each cross-correlation at 8, 14, 25 and 50 sec period in northern winter and northern summer of 2004. Each line points in the direction from which the energy arrives (i.e., it points to the source) and its length is proportional to the SNR. At 8 and 14 sec period, lines drawn to the edge of circle represent a SNR of at least 80, and at 25 sec and 50 sec the lines to the circle's edge mean the SNR is at least 60.

The periods of 8 and 14 sec are near the center of the secondary (5-10 sec) and primary (10-20 sec) microseism bands, respectively. The strength and directionality of ambient noise at these two periods are shown in Figure 5 to be very similar to one another, and they demonstrate similar, strong seasonal dependence with much stronger noise arriving in the northern winter than in the northern summer. The seasonal variation in the strength of ambient noise, with the noise level being much higher in winter than in summer, is consistent with higher sea states in winter than in summer in the north Atlantic [*Webb*, 1998]. In the winter, at both periods the strongest energy is arriving from the northwest quadrant. The strongest arrivals are also from the northwest quadrant during the summer, but the arrivals from the north are less energetic. The one exceptional difference between the patterns of energy arrival at 8 and 14 sec is stronger noise from the northeast quadrant at 14 sec period during the northern summer.

The patterns of energy arriving at the longer periods of 25 and 50 sec period are quite distinct from waves in the microseism band. These waves display little seasonal variability and the azimuthal patterns of energy arriving at these periods are very similar, with the strongest energy arriving from the northeast at both periods and seasons. The

only appreciable difference between 25 and 50 sec is that the SNR at 25 sec is higher than at 50 sec period.

Figures 6 and 7 illustrate possible source locations by back-projecting a great-circle arc for each station-pair with a SNR > 20. In the secondary microseism band (~8 sec period) shown in Figure 6, source directions are broadly distributed to the west and northwest of Europe. The simplest distribution of source locations would be for them to occur near the European coast, ranging from west of Spain to the European Arctic coast of the Baltic peninsula in winter. The alternative would be for the sources to emanate from a much larger area, to lie in deep water spanning the entire North and Central Atlantic. We view this as implausible. In northern summer, the range of azimuths for the high SNR sources diminishes to near coastal France, England, the North Sea region, and coastal Norway. At 14 sec period during the summer, seismic energy also arrives to the European stations from the northeast, apparently having emanated from east of Asia. Again, the simplest explanation would be for the sources to occur along the east Asian coastline, predominantly off of China, Korea/Japan, and Russia. The sole significant difference between 8 and 14 sec period is these arrivals from the east Asian coast at 14 sec during the northern summer. This can be understood as a wave propagation phenomenon, with the 8 sec waves having been attenuated more than those at 14 sec.

At 25 sec and 50 sec, illustrated in Figure 7, the patterns of the back-projected rays are nearly identical with each other and in summer and winter. The strongest arriving energy is from the northeast, probably having originated along the western Pacific coast-lines. Again, we view the shallow water source location to be more plausible than the deep water sources distributed over a much larger area. There are fewer large amplitude arrivals from the western quadrants. Those that exist probably have originated near the European coast. Although deep water sources for the longer period arrivals cannot be ruled out on the basis of the seismic evidence alone, the spatial distribution of sources would have to be very diffuse and this seems to us to be unlikely.

Our analysis of ambient noise directionality in Europe indicates little significant difference between the directional content of energy arriving in the two microseism bands. The differences that do exist can be attributed to the fact that the longer period primary microseismic energy (~14 sec) propagates farther than secondary microseismic energy (~8 sec). In addition, the principal of simplicity argues for near-coastal source locations. However, the method we use cannot locate noise sources unambiguously, and the results in Europe may differ from those elsewhere in the world. Thus, in the following sections, we analyze ambient noise directionality in southern Africa, Tibet, and North America.

4. Further analysis: Cross-correlations of ambient noise in southern Africa and Asia

The stations used in this analysis are shown in Figure 8. Twelve-months of data are processed using stations from two PASSCAL experiments; the Southern Africa Seismic Experiment (SASE) with data from 1998 and the Eastern Syntaxis Tibet Experiment with data from 2003 and 2004. We process data exactly as for the European stations, but obtain results only at period of 8, 14 and 25 sec because the arrays are smaller and longer period results are less robust than in Europe. The azimuthal distribution of SNR from the southern African, Tibetan, and European stations are plotted in Figure 9 in both the northern summer and winter.

Like in Europe, at 8 and 14 sec period, considerable seasonal variability is observed both in southern Africa and Tibet. In Tibet, ambient noise is stronger in the northern winter than the northern summer and the principal directions of noise swing to the south in the northern summer. In understandable contrast to the observations in Europe, however, ambient noise is stronger at these periods in southern Africa during the northern summer (southern winter) than in the northern winter (southern summer) (Fig. 9a-d). Thus, at 8 and 14 sec period, ambient noise is stronger in the local winter in most directions in all three locations. In southern Africa, the azimuthal content of noise emanating from the southern quadrants at these two periods is very similar to one another

and there is less seasonal dependence. The simplest explanation is that ambient noise from the southern quadrants arrives from nearby coastlines having been generated there. Noise from the northern quadrants in southern Africa is different at 8 and 14 sec, however, and there is a stronger seasonal dependence. Strong noise (SNR > 40) at 14 sec arriving from the north and northwest to southern Africa during the northern winter, back-projects to the northern European coasts, similar to observations in Europe. Strong noise (SNR > 60) arriving at 14 sec from the northeast, which is particularly strong in the northern summer, is more difficult to interpret. For example, as shown in Figure 9d, this noise back-projects to the east Asian coast similar to results from the European stations, but the Tibetan results indicate that the strongest noise there is coming from the southwest rather than the northeast. It is unlikely, therefore, that the strong arrivals at 14 sec observed at the European and southern African stations emanate from a single source region in east Asia. We believe that it is more likely that the 14 sec southern African energy finds its source near the African coast or perhaps along the coastlines of the Arabian Sea.

These observations illustrate that the azimuthal patterns of microseismic energy arriving at these three locations display some common systematics, particularly as related to seasonal variability. Differences between the 8 sec and 14 sec observations again can be understood largely as propagation effects. The source locations of the noise arriving in these regions are largely distinct, however. It is, therefore, unlikely that large storms in the deep oceans are the direct source of microseismic energy at 14 sec period, which is more likely to have been produced in relatively shallow near coastal waters. The seasonal variability of the microseisms, however, illustrates that large deep ocean storms are probably the cause of the ocean gravity wave energy that transforms to ambient seismic noise in shallow waters.

At 25 sec period, as in Europe, there is little seasonal dependence of the directionality of ambient noise in southern Africa and the azimuthal content of ambient noise at this period differs substantially with that at either 8 sec or 14 sec period. The

southern African noise at this period is generally of larger amplitude than in Europe, probably due to higher sea states in the southern hemisphere, and is also more omni-directional than in Europe, consistent with the source of the ambient noise occurring near the coast along much of southern Africa rather than in deep water to the south of Africa where sea-states are highest. In Tibet, like Europe and southern Africa, the azimuthal distribution of incoming noise at 25 sec differs substantially from 8 or 14 sec period. But, unlike Europe or southern Africa, there is substantial seasonal variability, with strong noise coming from the southern quadrants in both the northern summer and winter but also from the north in the northern winter. The directions of arrival of strong noise in Europe, southern Africa, and Tibet at 25 sec are not consistent with a single or small number of exceptionally strong source locations, but rather indicate that strong noise emerges at these arrays from many directions, presumably with a broad distribution of source locations. These observations are, therefore, at variance with a deep water source for ambient noise at 25 sec period.

5. Further analysis: Cross-correlations of ambient noise in North America

We also use continuous seismic data from numerous stations in California, the eastern US, Alaska and northwest Canada, processeding them using the same methods as for the European, southern African, and Tibetan data. The stations are shown in Figure 10 and the results are presented at 8, 14, and 25 sec in Figure 11.

At 8 and 14 sec period, results for the stations in the eastern US and Alaska/Canada are straightforward. SNR is larger in the northern winter than the northern summer, but the directional dependence of noise is largely seasonally independent. In addition, the directional patterns at these periods are largely similar. In Alaska/northern Canada, ambient noise at these periods arrives mainly from the south, presumably along the Pacific coast of Canada and Alaska. In the eastern US, in contrast, ambient noise arrives mainly from the northeast and west; i.e., either from the Canadian Atlantic coast or the

Pacific coast of North America. Thus, at these locations there is no evidence of significant differences in the source locations at 8 and 14 sec period.

In the microseismic bands in California, the results are somewhat more complicated, however. At 8 sec, there is weak seasonal variability with stronger waves arriving from the northwest in winter than in summer. At 14 sec the seasonal variation is strong and the 8 sec and 14 sec azimuthal patterns differ from one another. In the northern winter, the strongest signals arrive to California from the northwest and northeast at 14 sec, presumably arriving from the northern Pacific and northern Atlantic coasts of North America. In the northern summer, however, the strongest arrivals are from the south and southwest, with the source locations probably being localized to the nearby coasts. These patterns are different from those at 8 sec period, in which the dominant arrivals are in the southwest quadrant throughout the year, similar to the azimuthal distribution at 14 sec period during the northern summer. *Stehly et al.* [2006] argue from a similar observation for the physical decoupling of the primary and secondary microseisms. We believe a much more simple explanation is that these arrivals at 14 sec period are coming from North American coast-lines in the North Pacific and North Atlantic which are too far to be observed well at 8 sec period.

At 25 sec across North America, the azimuthal patterns are largely seasonally invariant with the most energic waves apparently coming from the Pacific coast of the western US.

Thus, from microseismic band to long-period ambient noise in North America, these results are consistent with near-coastal sources similar to our observations in the eastern hemisphere. The observed differences in directivity at 8, 14 and 25 sec can be attributed to propagation and attenuation, rather the generation mechanism.

6. Azimuthal coverage and recovery of empirical Green's functions

In most theoretical treatments of ambient noise tomography and coda wave

interferometry, the assumption of a perfectly homogeneous distribution of noise sources is made [e.g., *Snieder*, 2004]. The observed distribution of ambient noise is far from homogeneous, however, with exceptionally strong signals sometimes emanating only from a narrow range of azimuths. Therefore, a question has been raised [e.g., *Rhie and Romanowicz*, 2006] about the effect that this will have on the emergence of accurate Green's functions from cross-correlations of ambient noise and whether the observations can be used meaningfully to obtain dispersion measurements and perform tomography.

This question has been addressed observationally in previous studies [e.g., *Shapiro et al.*, 2005; *Yang et al.*, 2007a; *Lin et al.*, 2007b; *Moschetti et al.*, 2007; *Bensen et al.*, 2007a,b) using several lines of evidence. These studies showed that the observed inter-station Green's functions are similar to earthquake signals when earthquakes occur near to one of the stations, that dispersion curves are seasonally repeatable even though ambient noise characteristics may change substantially, and that the dispersion curves are consistent with one another even when azimuths are quite different. In addition, they showed that the resulting group and phase velocity maps reproduce geological structures faithfully. These and other reasons help to establish the veracity of ambient noise tomography. It should be borne in mind, however, that considerable efforts are exerted in processing ambient noise data to identify bad measurements (commonly more than half of all observations), some of which result from low signal levels or incomplete constructive/destruction interference in the generation of the observed Green's functions.

The apparent veracity of ambient noise tomography appears, however, to be in conflict with the existence for relatively narrow azimuthal ranges with extraordinarily large amplitudes of ambient noise (e.g., Figure 12a-c). Figure 12d-f, which presents histograms of the number of 12-month European inter-station cross-correlations with SNR > 10 on either the positive or negative component, illustrates why this is not contradictory. The reason is that signals with SNR > 10 emerge from a wide range of azimuths. Only the very strongest signals are azimuthally limited. Thus, although there

are preferred directions for ambient noise, predominantly at very short periods, significant ambient noise signals exist at a wide range of azimuths.

In order to demonstrate that accurate empirical Green's functions are obtained from long time noise series when ambient noise sources have an inhomogeneous azimuthal distribution with strong sources in some preference directions, we present three synthetic experiments with different noise energy distributions. Synthetic sources are randomly distributed in a circular region with a diameter of 4000 km and a pair of stations are placed 450 km apart (Figure 13a). Each synthetic source emits a wavelet at a random initial time and at a random location. The waveform of the wavelet is the second derivative of a Gaussian function with a 20 second standard deviation. The wave velocity inside the circular region is 3 km/s everywhere. For each experiment, we run 30 simulations for each individual day totaling 30 days. For each day, 6000 sources are randomly distributed, but source energy has an azimuth-dependent distribution as shown in Figure 13b-d. The resulting cross-correlations are 30-day stacks. The empirical Green's functions, which are the negative time derivatives of the resulting cross-correlations (Snieder, 2004), are plotted in Figure 14a with the theoretical Green's function plotted at the bottom as comparison.

In experiment I, the distribution of sources is azimuthally homogenous. Thus, the cross-correlation is nearly symmetric. In experiment II, there is stronger source energy coming from right, which makes the cross-correlations highly asymmetric with a much higher signal-noise-ratio on the positive component. In experiment III, stronger source energy comes from the northeast direction. The resulting cross-correlation is nearly symmetric because the strong sources from the northeast interfere with each other destructively. The arrival times of the peak energy at both positive and negative lags of the three cross-correlations are about 150 sec, which is the time for the wave to propagates between the two stations. We follow *Lin et al.* [2007b] and obtain phase velocity measurements for the retrieved cross-correlations by automatic frequency-time

analysis (FTAN). The measured phase velocities and travel times are close to the input phase velocity (3 km/s) and travel time (150 sec) at all periods with errors less than about 0.5% at all periods (Figure14 b and c). The maximum travel time error (<2/3 sec) is less than measurements errors with real data and considerably less than the RMS of data misfit in ambient noise phase velocity tomography [*Yang et al.*, 2007b; *Lin et al.*, 2007b].

These three synthetic experiments show that if ambient noise exists over a broad azimuthal range even at relatively low levels, accurate empirical Green's functions will emerge from long time series of the ambient noise.

With the results from the synthetic experiments in mind, Figure 12g-i provides additional insight into why ambient noise tomography works so well. It presents bearing angles of path segments for the selected cross-correlations at periods of 10, 16 and 30 sec. Bearing angles are defined only between azimuthal angles from -90^{o} and 90^{o} because, for any cross-correlation, positive and negative components with noise coming from two opposite directions have the same bearing angle. Although there is a slight preponderance of paths striking northwest-southeast across Europe, particularly at short periods, the distribution is strikingly homogeneous, which is good for the emergence of accurate empirical Green's functions and for resolution in surface wave tomography, particularly for extracting information about azimuthal anisotropy. These observations provide another line of evidence that highlights the advantage of ambient noise in providing homogenous ray coverage in surface wave tomography.

7. Conclusions

Three principal questions have motivated this study. (1) Are the primary and secondary microseisms physically decoupled? (2) Is ocean-produced ambient seismic noise generated in relatively shallow near-coastal waters or in deep water at long periods? (3) Is the azimuthal distribution of ambient noise sufficiently homogeneous to allow for the retrieval of largely unbiased empirical Green's functions? We addressed each of these

questions by investigating the strength and azimuthal distribution of ambient noise between 8 and 50 sec period in Europe, southern Africa, Tibet, and three regions in North America (California, Alaska/northern Canada, eastern US). Because the methods we use recover information only about the direction to strong ambient noise sources and not their absolute locations, the results are not entirely unambiguous. The inferences that we draw, therefore, are based also on appealing to the principle of simplicity.

First, we find no compelling evidence for the physical decoupling of the primary and secondary microseisms. The seasonal variation of the two microseisms is similar in all regions that we studied. Although the azimuthal distributions of the two microseisms do vary in some places, this difference is most simply attributable to the fact that the primary microseism can propagate coherently over much longer distances than the secondary microseism. It is possible and probably likely, however, that the relative amplitude of the primary and secondary microseisms upon generation of these waves is globally variable. But, characterizing the regional variation of this ratio is beyond the scope of this paper.

Second, in all studied regions and at all periods studied here (8 – 50 sec) the most simple location for the source of ambient noise lies in near-coastal waters. Deep water sources cannot be formally ruled out by the methods we apply here. We show, however, that deep water source regions would have to cover much of the ocean basins, which we argue is unlikely.

Third, and perhaps surprisingly, ambient noise emerges in each of the studied regions at a broad range of azimuths. If this does appear surprising it is probably because studies of ambient noise typically have focused on characterizing the strongest ambient noise directions, which are limited in azimuth. Even though the strongest noise emerges only

from a few directions in most places, strong ambient noise emerges from many directions. Thus, for the orientation of most station-pairs, sufficiently strong ambient noise is present to be the basis for the retrieval of reliable empirical Green's functions. Nevertheless, there are some azimuths in most regions where ambient noise is so weak that inter-station cross-correlations will not provide a good empirical Green's function. From a practical perspective, therefore, these cross-correlations have to be identified and removed as candidate empirical Green's functions. Typically, these cross-correlations have a low signal-to-noise ratio, and SNR is useful in the data processing part of ambient noise tomography to identify the acceptable empirical Green's functions [e.g., *Bensen et al*, 2007a]. The principal caveat is that there are some exceptionally strong spurious signals, such as the persistent 26 sec resonance in the Gulf of Guinea [*Shapiro et al.*, 2006)], that require dedicated data processing to remove [*Bensen et al.*, 2007a].

In closing, the ways in which the strength and distribution of ambient noise vary in both azimuth and region appear to be consistent generally with the hypothesized generation of ambient noise advocated by *Rhie and Romanowicz* [2006]. In this scenario, wind energy is converted to ocean wave energy in the deep oceans. Ocean wave energy is then transported to the fringes of continents as ocean gravity waves (or so-called infragravity waves at longer periods). Near coast-lines, ocean gravity waves convert to solid-earth propagating seismic waves when water is shallow enough to allow their direct interaction with the seafloor. The primary and secondary microseisms are physically coupled through a non-linear, frequency-doubling process resulting from wave-wave interactions between the direct and coastally reflected waves. It may not be generally appreciated that this mechanism would predict that ambient noise is well distributed in azimuth. Ocean gravity waves generated in deep water will propagate to coast-lines broadly across the ocean basin where seismic waves will be generated over a large area in relatively shallow water. This mechanism also would predict that the strongest seismic waves would be generated

when and where the storm intersects the coast-line. Both of these predictions, the broad area of generation of ambient noise along coast-lines and the strongest waves emanating from only a few azimuths, are consistent with our observations. Given the ambiguities inherent in the methods applied herein, however, we view these results as relatively weak confirmation of the hypothesized mechanism of Rhie and Romanowicz. More direct observations are needed to test this hypothesis further.

Acknowledgments

The data used in this research were downloaded from the continuous ftp database of the Orfeus (Observatories and Research Facilities for European Seismology) Data Center and from the IRIS Data Management Center. The authors are deeply grateful to the networks that contribute data to the Virtual European Broadband Seismic Network (VEBSN), a partnership of more than 30 local, regional and global arrays and networks. In addition, the authors would like to acknowledge two PASSCAL experiments that provided data for this research: the Southern Africa Seismic Experiment and the Eastern Syntaxis Tibet Experiment. This research was supported by US National Science Foundation grant EAR0711526 and US Department of Energy contract DE-FC52-2005NA26607.

References

Aki, K. and B. Chouet (1975), Origin of coda waves: source, attenuation, and scattering effects, *J. Geophys. Res.*, 80, 3322-3342.

Bensen, G.D., M.H. Ritzwoller, and N.M. Shapiro (2007b), Broad-band ambient noise surface wave tomography across the United States, submitted to *J. Geophys. Res.*

Bensen, G.D., M.H. Ritzwoller, M.P. Barmin, A.L. Levshin, F. Lin, M.P. Moschetti, N.M. Shapiro, and Y. Yang (2007a), Processing seismic ambient noise data to obtain

reliable broad-band surface wave dispersion measurements, *Geophys. J. Int*., doi: 10.1111/j.1365-246X.2007.03374.x.

Cho, K. H., R. B.Herrmann, C. J.Ammon, K, Lee (2007), Imaging the Upper Crust of the Korean Peninsula by Surface-Wave Tomography, *Bull. Seism. Soc. Am.*, 97,198-207.

Derode, A., E. Larose, M. Campillo, and M. Fink (2003), How to estimate the Green's function of a heterogeneous medium between two passive sensors? Application to acoustic waves, *Appl. Phys. Lett.*, 83, 3054-3056.

Ekstrom, G. (2001), Time domain analysis of Earth's longperiod background seismic radiation, *J. Geophys. Res*., 106, 26,483–26,493.

Gudmundsson, O., A. Khan, and P. Voss (2007), Rayleigh-wave group-velocity of the Icelandic crust from correlation of ambient seismic noise, *Geophys. Res. Lett.*, 34, L14314, doi:10.1029/2007GL030215.

Hasselmann, K. (1963), A statistical analysis of the generation of microseisms, *Rev. Geophys*., 1, 177–210.

Lin, F., M.H. Ritzwoller, J. Townend, M. Savage, S. Bannister (2007a), Ambient noise Rayleigh wave tomography of New Zealand, *Geophys. J. Int*.., 18 pages, doi:10.1111/j.1365-246X.2007.03414.x.

Lin, F., M.P. Moschetti, and M.H. Ritzwoller (2007b), Surface wave tomography of the western United States from ambient seismic noise: Rayleigh and Love wave phase velocity maps, *Geophys. J. Int.*, submitted.

Longuet-Higgins, M. S. (1950), A theory on the origin of microseisms, *Philos. Trans. R. Soc. London*, 243, 1–35.

Moschetti, M.P., M.H. Ritzwoller, and N.M. Shapiro (2007), Surface wave tomography of the western United States from ambient seismic noise: Rayleigh wave group velocity maps, *Geochem., Geophys., Geosys.*, 8, Q08010, doi:10.1029/2007GC001655.

Nawa, K., N. Suda, Y. Fukao, T. Sato, Y. Aoyama, and K. Shibuya (1998), Incessant

excitation of the Earth's free oscillations, *Earth Planets Space*, 50, 3–8.

Paul, A. M. Campillo, L. Margerin, E. Larose, and A. Derode (2005), Empirical synthesis of time-asymmetrical Green functionGreen's functions from the correlation of coda waves, *J. Geophys. Res.*, 110, B08302, doi:10.1029/2004/JB003521.

Rhie, J., and B. Romanowicz (2004), Excitation of Earth's continuous free oscillations by atmosphere-ocean-seafloor, *Nature* 431, 552-556.

Rhie, J., and B. Romanowicz (2006), A study of the relation between ocean storms and the Earth's hum, *Geochem,. Geophys,. Geosyst*., 7, Q10004, doi:10.1029/2006GC001274.

Sabra, K. G., P. Gerstoft, P. Roux, W. A. Kuperman, and M. C. Fehler (2005), Surface wave tomography from microseism in southern California, *Geophys. Res. Lett.*, 32, L14311, doi:10.1029/2005GL023155.

Shapiro, N.M. and M.H. Ritzwoller (2002), Monte-Carlo inversion for a global shear velocity model of the crust and upper mantle, *Geophys. J. Int.*, 151, 88-105.

Shapiro, N.M. M. Campillo, L. Stehly, and M.H. Ritzwoller (2005), High resolution surface wave tomography from ambient seismic noise, *Science*, 307, 1615-1618.

Shapiro, N.M., M.H. Ritzwoller, and G.D. Bensen (2006), Source location of the 26 sec microseism from cross correlations of ambient seismic noise, *Geophys. Res. Lett.*, 33, L18310, doi:10.1029/2006GL027010.

Snieder, R., (2004) Extracting the Green's function from the correlation of coda waves: A derivation based on stationary phase, *Physical Review E*, 69, 046610.

Stehly, L., M. Campillo, N.M. Shapiro (2006), A study of the seismic noise from its long range correlation properties, *J. Geophys. Res.* 111, B10306, doi:10.1029/2005JB004237.

Tanimoto, T. (2005), The oceanic excitation hypothesis for the continuous oscillations of the Earth, *Geophys. J. Int*., 160, 276–288.

Tanimoto, T., and J. Um (1999), Cause of continuous oscillations of the Earth, *J.*

Geophys. Res., 104, 28,723–28,739.

Webb, S. C. (1998), Broadband seismology and noise under the ocean, *Rev. Geophys*. 36, 105-142.

Yang, Y., M.H. Ritzwoller, A.L. Levshin, and N.M. Shapiro (2007a), Ambient noise Rayleigh wave tomography across Europe, *Geophys. J. Int.*, 168, 259-274.

Yang, Y., A. Li, and M.H. Ritzwoller (2007b), Crustal and uppermost mantle structure in southern Africa revealed from ambient noise and teleseismic tomography, submitted to *Geophys. J. Int.*

Yao, H., R.D. van der Hilst and M.V. De Hoop (2006), Surface-wave array tomography in SE Tibet from ambient seismic noise and two-station analysis: I - Phase velocity maps, *Geophys. J. Int.*, 166, 732-744.

Figure captions

Figure 1. Broadband seismic stations in Europe used in this study, marked by red triangles.

Figure 2. Examples of some 12-month broadband cross-correlations. The bold gray line indicates the zero arrival time. Cross-correlations are ordered by intra-station distances with station names indicated in each waveform panel. Note that some cross-correlations are often asymmetric. The bottom map shows the locations of stations (white triangles) and path segments for corresponding cross-correlations with arrows marking incoming directions of noise contributing to positive components.

Figure 3. Normalized spectrums of positive (right) and negative (left) components of

cross-correlations shown in Fig.2. The three frequency bands of LFN, MS1 and MS2 delineated by the bold lines correspond to the infragravity band, primary and secondary microseism bands.

Figure 4. (a) Example of a broadband positive-component cross-correlation using 12-months of data between stations IBBN (Ibbenbueren, Germany) and MOA (Molln, Austria). The broadband signal (5-150 sec) is shown at the bottom panel. Other panes are narrow band-pass filtered waveforms with central periods indicated in each panel. (b) Calculated SNR values for each narrow band-passed filtered waveforms versus period.

Figure 5. Azimuthal distribution of SNR of 5-month stacks during winter (left column) and summer (right column) at periods 8, 14, 25 and 50 sec taken from European seismic stations. SNR levels are indicted by the circles with values shown in each of the diagram.

Figure 6. Back-projected great-circle paths of cross-correlations at periods of 8 and 14 sec in summer and winter with corresponding azimuthal distribution over-plotted at the center of Europe. The great-circle paths indicate the approximate locations along which noise sources constructively contribute to surface wave signal. Paths shown here have SNR > 20.

Figure 7. Same as Fig. 6, but for periods of 25 and 50 sec.

Figure 8. Stations used in southern Africa from the Southern African Seismic Experiment and Tibet from the Eastern Syntaxis Tibet Experiment.

Figure 9. Similar to Fig. 6, but here the azimuthal distribution of SNR of 5-month stacks

during winter (left column) and summer (right column) at periods 8 (a and b), 14 (c and d), and 25 sec (e and f) in southern Africa and Tibet are compared with results from Europe. SNR levels in each region are indicted by the concentric circles that are scaled in multiples of 20. Paths in (d) are back-projected great-circle paths with SNR > 60.

Figure 10. Stations used in North America.

Figure 11. Same as Fig. 6, but for stations in the North America: California, the eastern US, and Alaska/Canada.

Figure 12. Azimuthal distributions (top) and histograms (middle) of the incoming directions of ambient noise as well as histograms (bottom) of bearing angles for cross-correlations with SNR>10 at 10, 16 and 30 sec. SNR levels are indicated by dashed circles with values shown.

Figure 13. (a) The circular region with a diameter of 4000 km for the noise simulation. Each red dot represents one of randomly distributed sources. The two blue triangles present two receivers placed 450 apart. (b), (c) and (d) The azimuthal distributions of the strength of source energy delineated by the bold lines for experiment I , II, and III, respectively.

Figure 14. (a) The empirical Green's functions from synthetic cross-correlations for experiment I, II and III. The bottom is the theoretical Green's function. (b) and (c) the phase velocity measurements and ,(d) and (e), travel times at various periods for the retrieved empirical Green's functions. The black line is for experiment I, the blue line for experiment II and the red lines for experiment III.

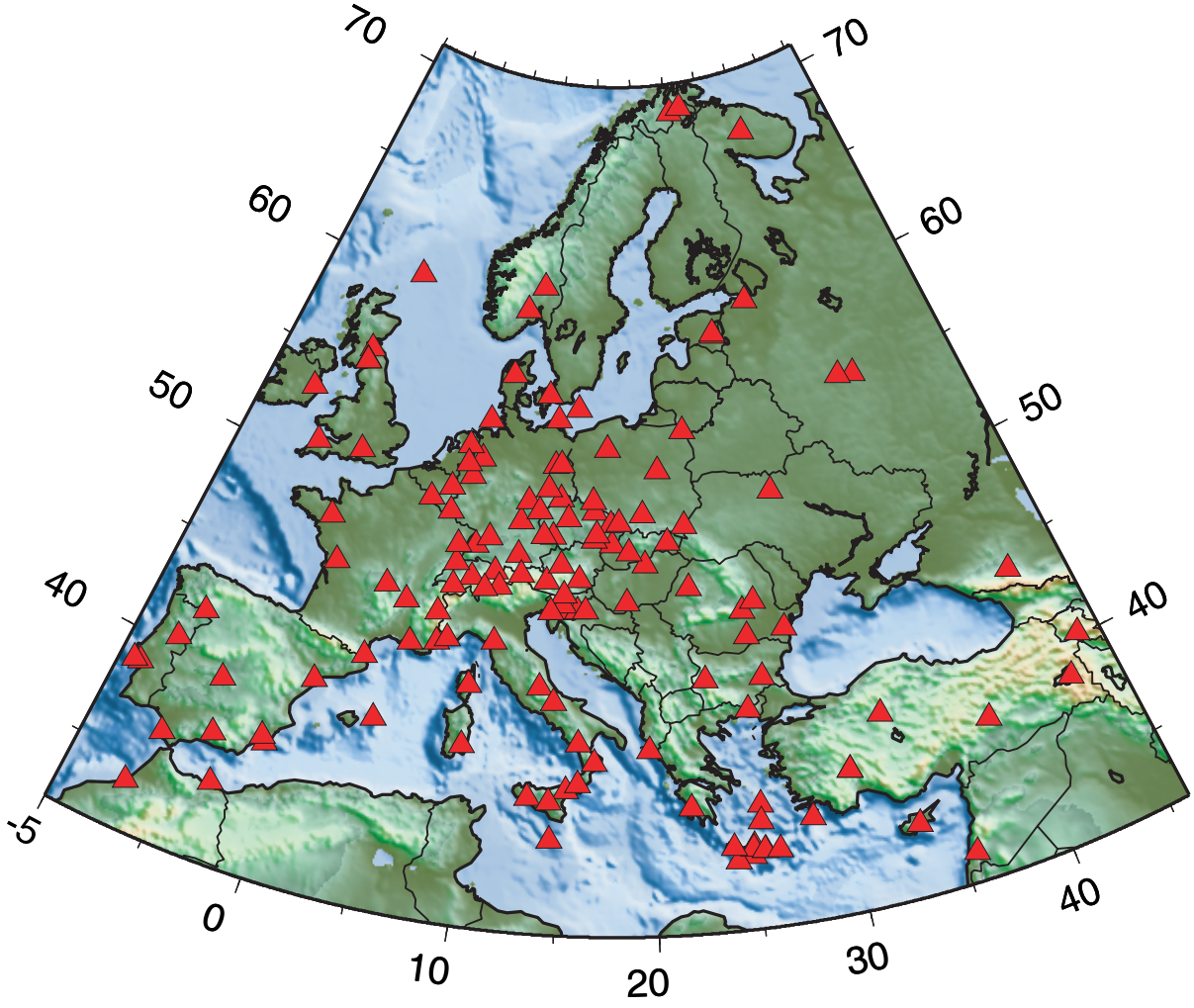
70
70
60
60
50
50
40
40
-5
0
10
20
30
40

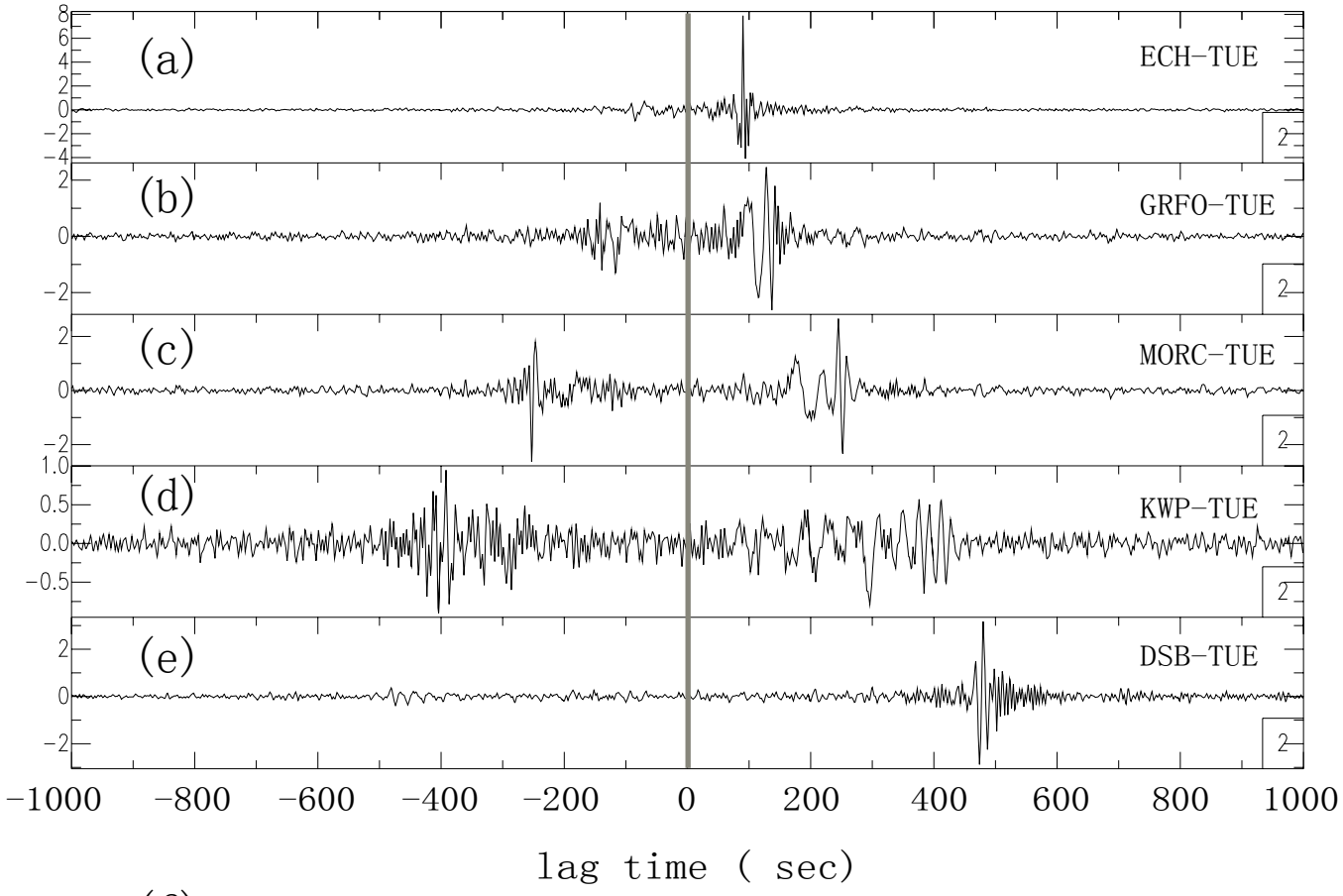
(a)
ECH-TUE
(b)
GRFO-TUE
(c)
MORC-TUE
(d)
KWP-TUE
(e)
DSB-TUE
−1000 −800 −600 −400 −200 0 200 400 600 800 1000
lag time (sec)

(f)

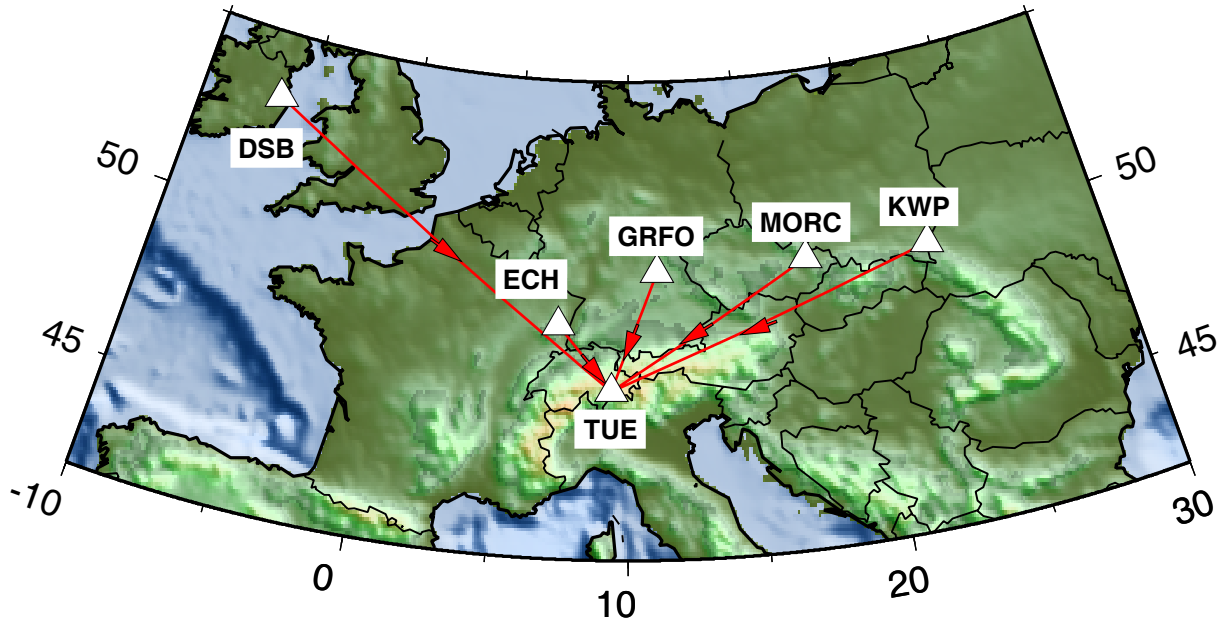
DSB
ECH
GRFO
MORC
KWP
TUE
50
45
-10
0
10
20
30

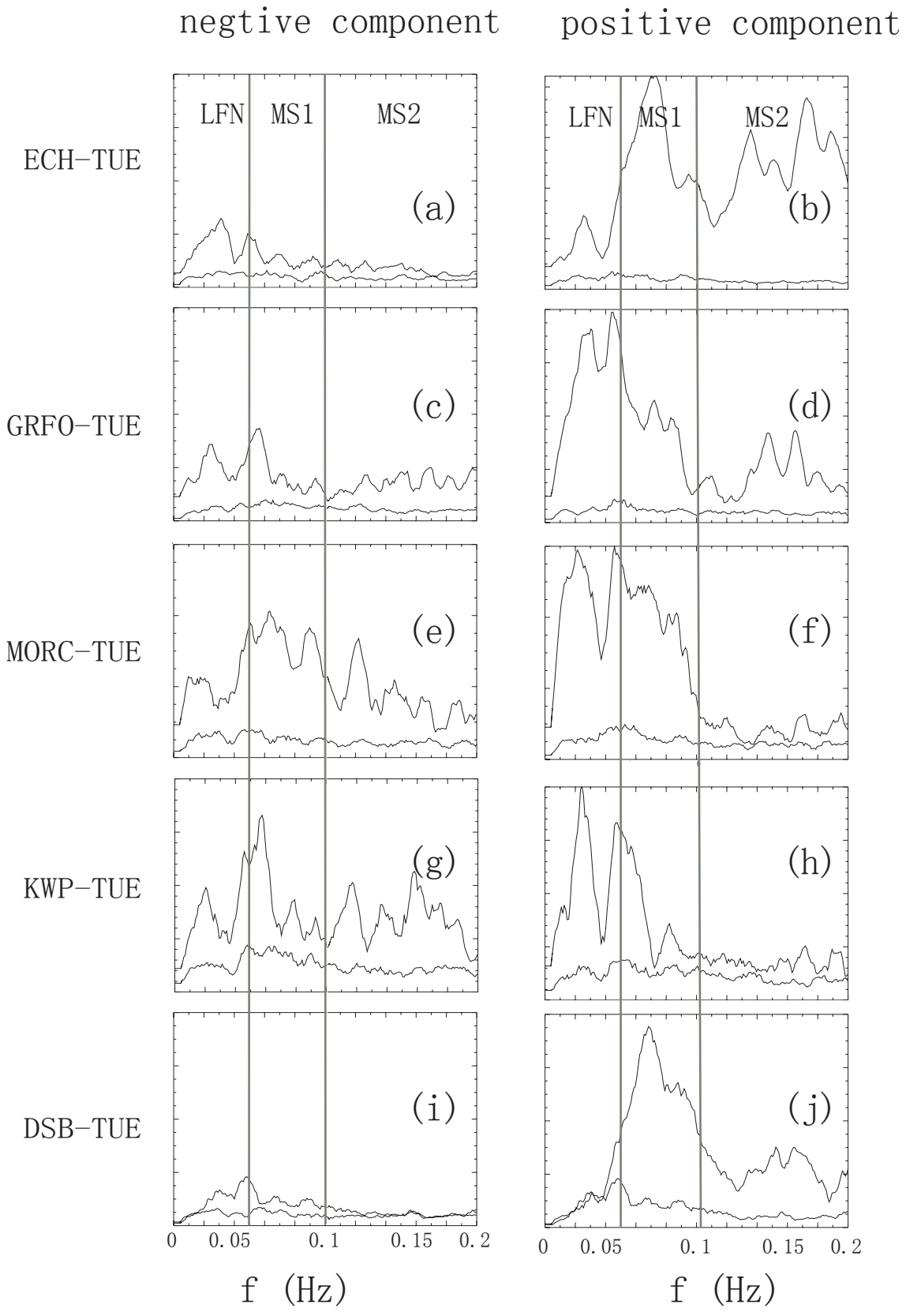
negtive component
positive component
ECH-TUE
GRFO-TUE
MORC-TUE
KWP-TUE
DSB-TUE
LFN
MS1
MS2
(a)
(b)
(c)
(d)
(e)
(f)
(g)
(h)
(i)
(j)
0
0.05
0.1
0.15
0.2
f (Hz)
f (Hz)

(a)

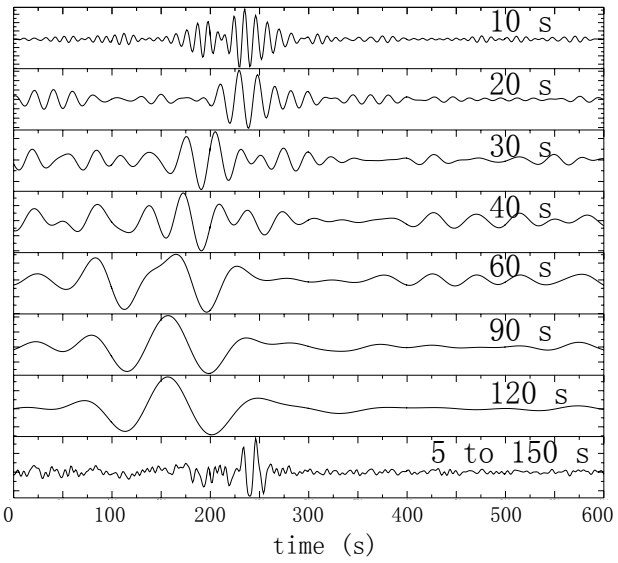
10 s
20 s
30 s
40 s
60 s
90 s
120 s
5 to 150 s
0
100
200
300
400
500
600
time (s)

(b)

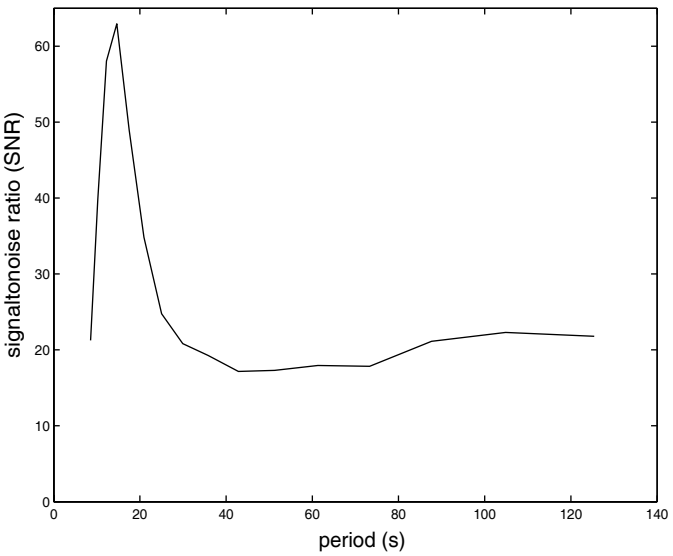
signaltonoise ratio (SNR)
0
10
20
30
40
50
60
0
20
40
60
80
100
120
140
period (s)

	northern winter	northern summer
8 sec	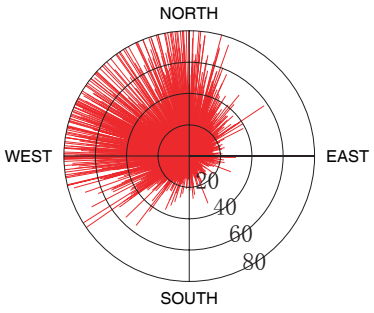	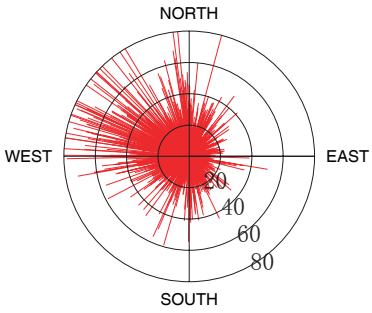
14 sec	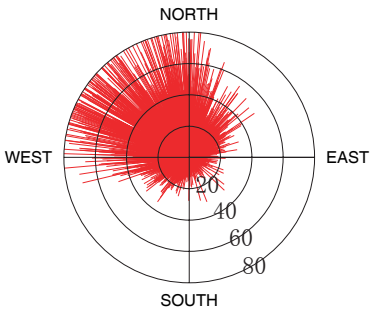	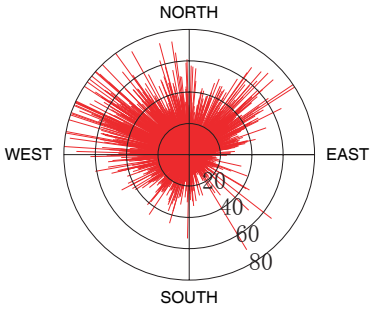
25 sec	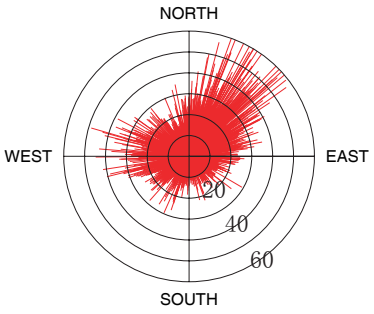	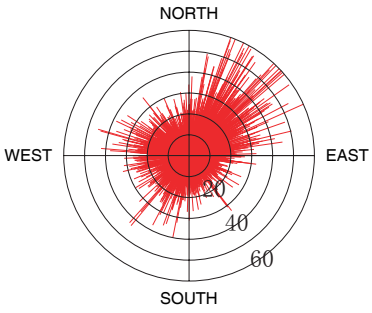
50 sec	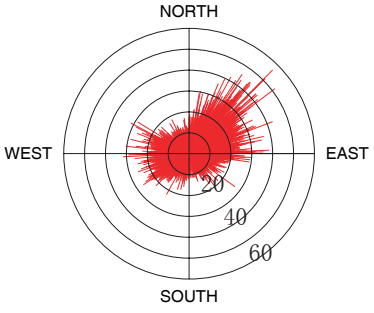	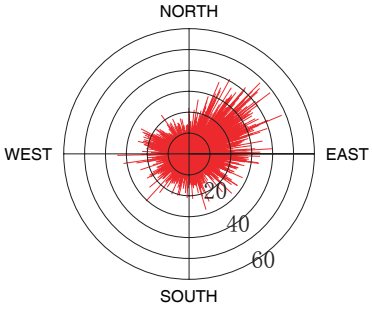

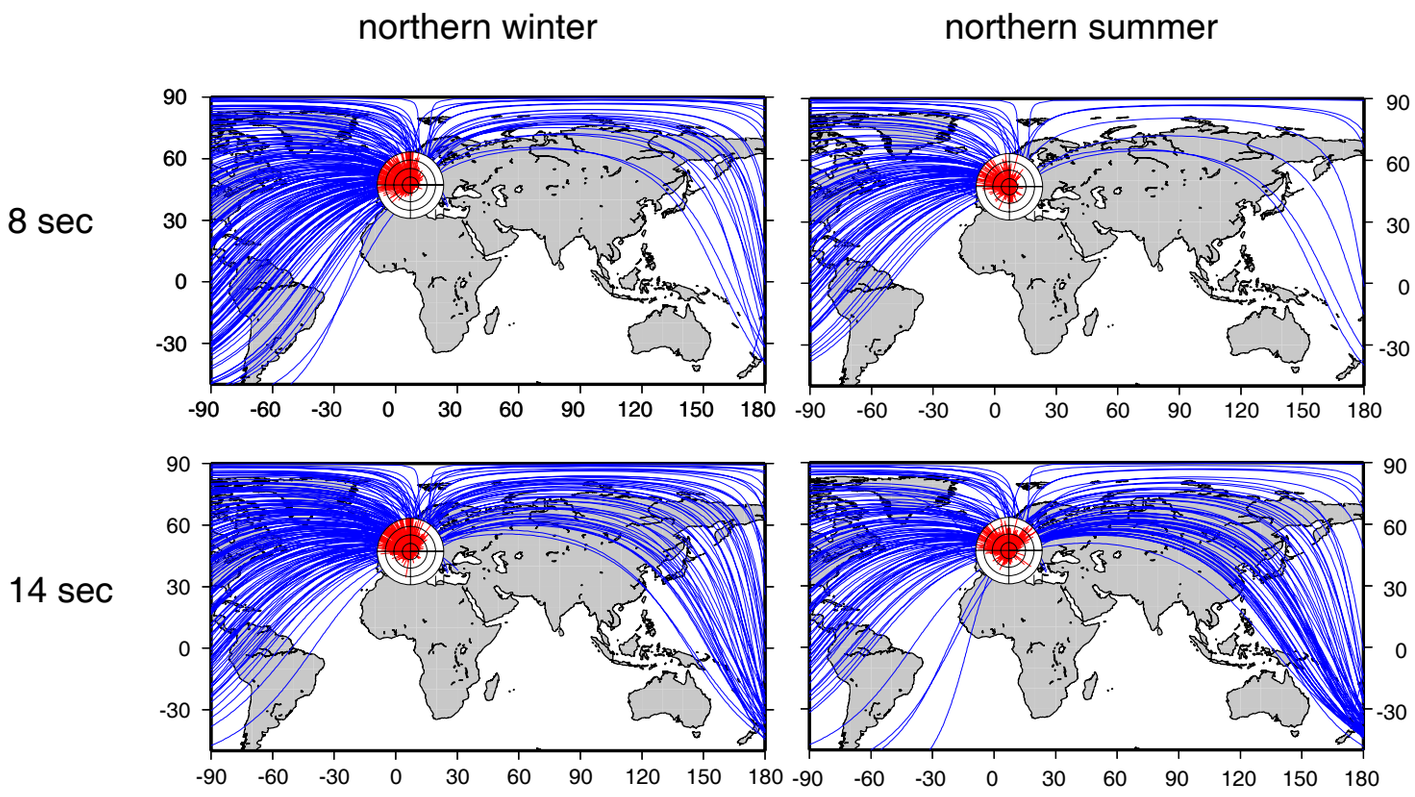
northern winter
northern summer
8 sec
14 sec
90
60
30
0
-30
-90 -60 -30 0 30 60 90 120 150 180

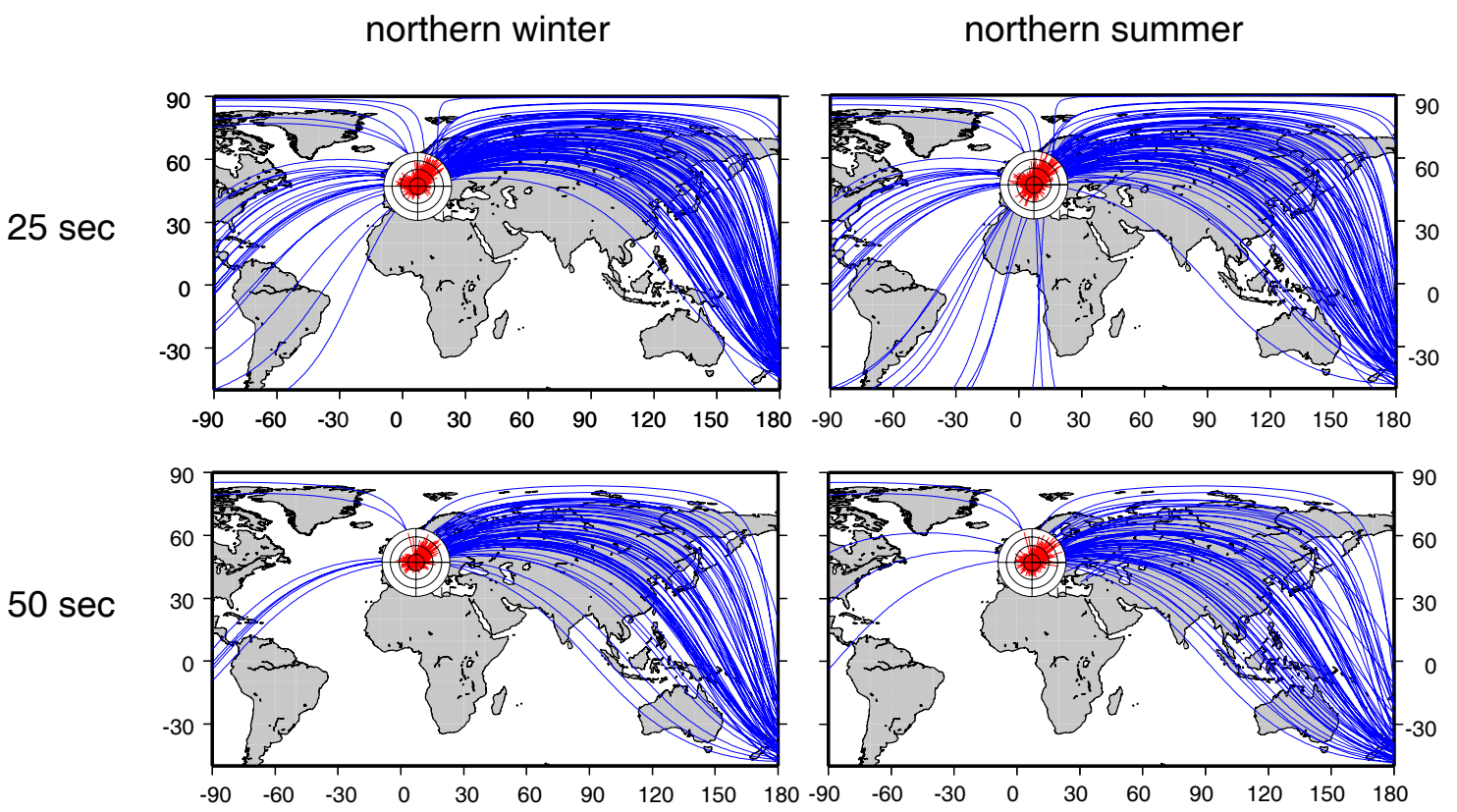
northern winter
northern summer
25 sec
50 sec
90
60
30
0
-30
-90 -60 -30 0 30 60 90 120 150 180

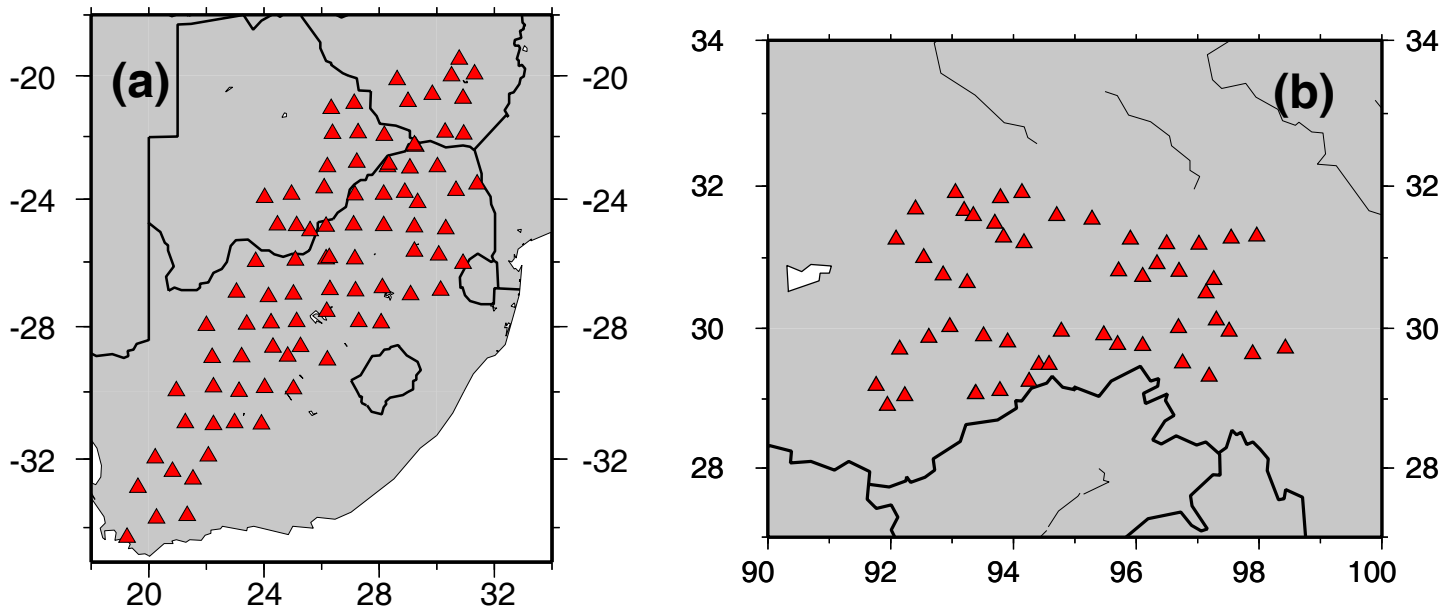
(a)
-20
-24
-28
-32
20
24
28
32
(b)
34
32
30
28
90
92
94
96
98
100

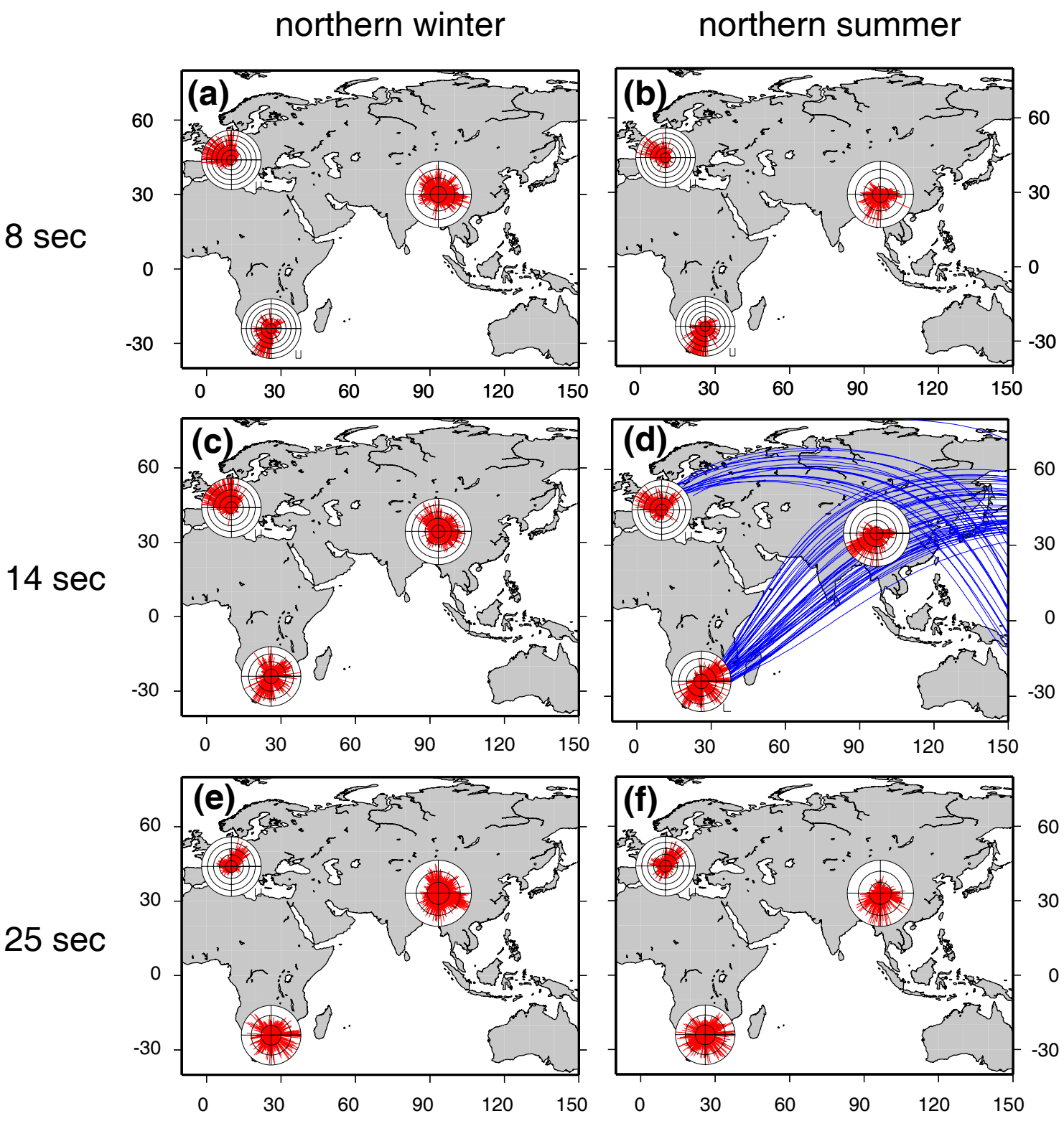
northern winter
northern summer
8 sec
14 sec
25 sec
(a)
(b)
(c)
(d)
(e)
(f)
60
30
0
-30
0
30
60
90
120
150

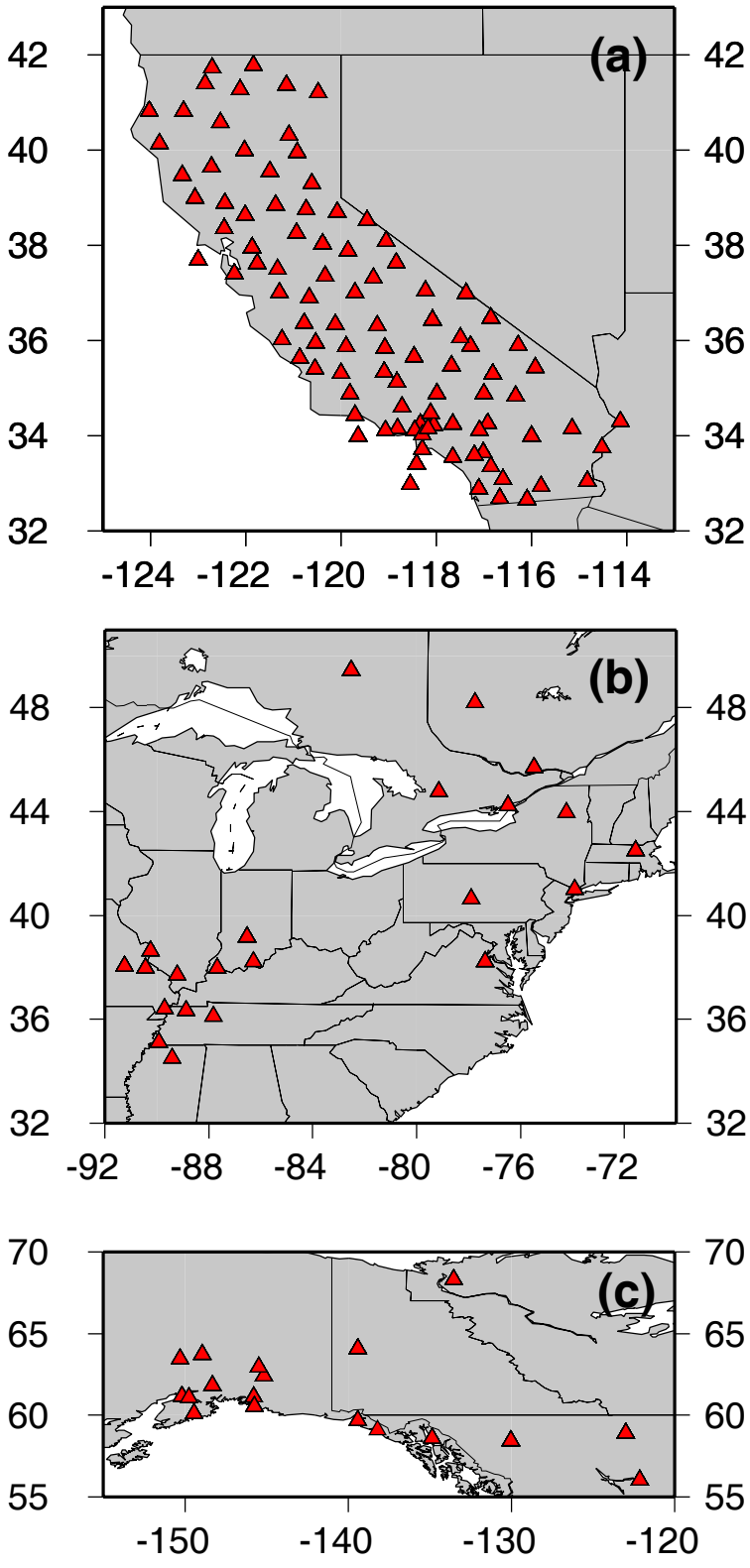
(a)
42
40
38
36
34
32
-124
-122
-120
-118
-116
-114
(b)
48
44
40
36
32
-92
-88
-84
-80
-76
-72
(c)
70
65
60
55
-150
-140
-130
-120

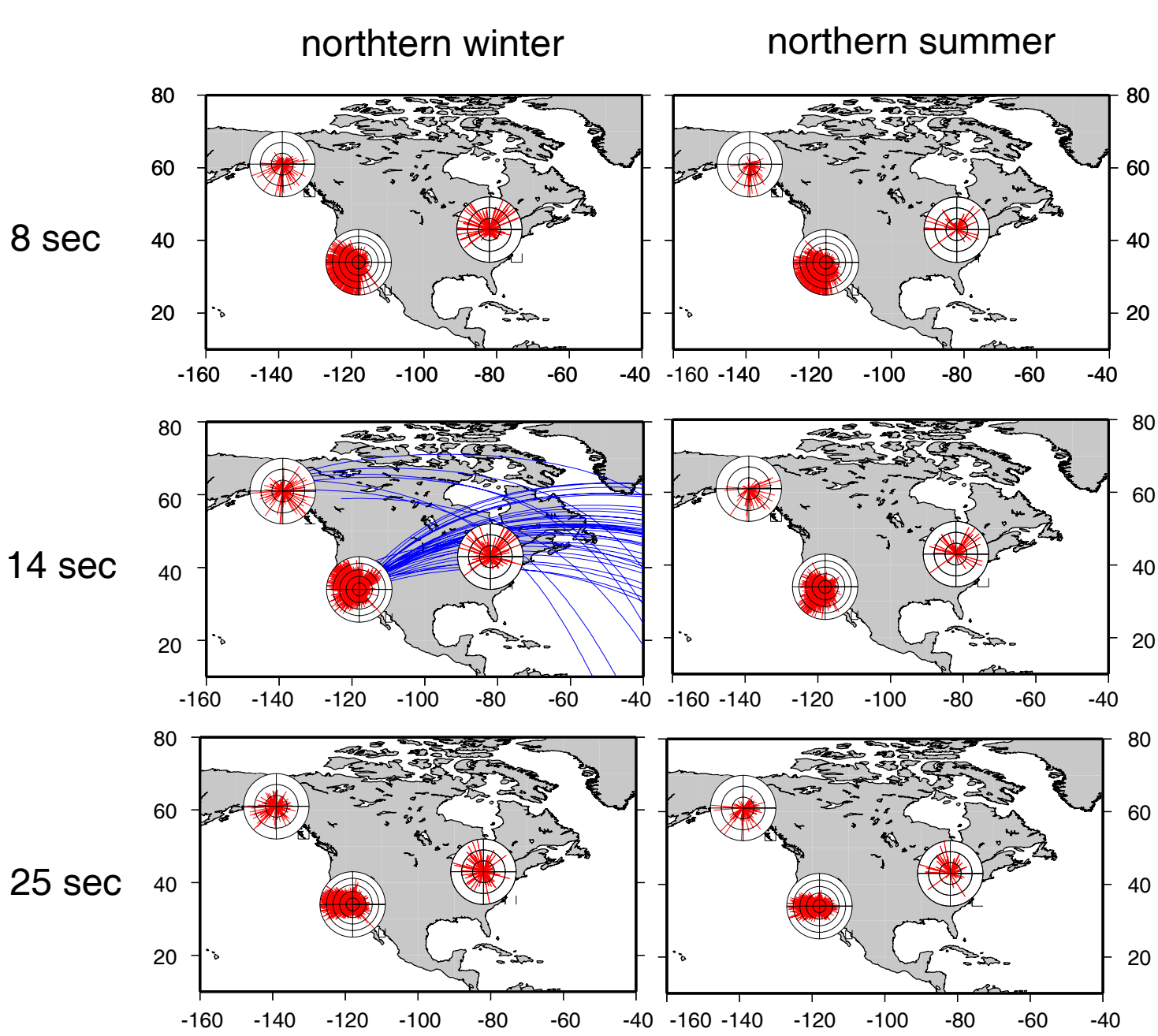
northtern winter
northern summer
8 sec
14 sec
25 sec
80
60
40
20
-160
-140
-120
-100
-80
-60
-40

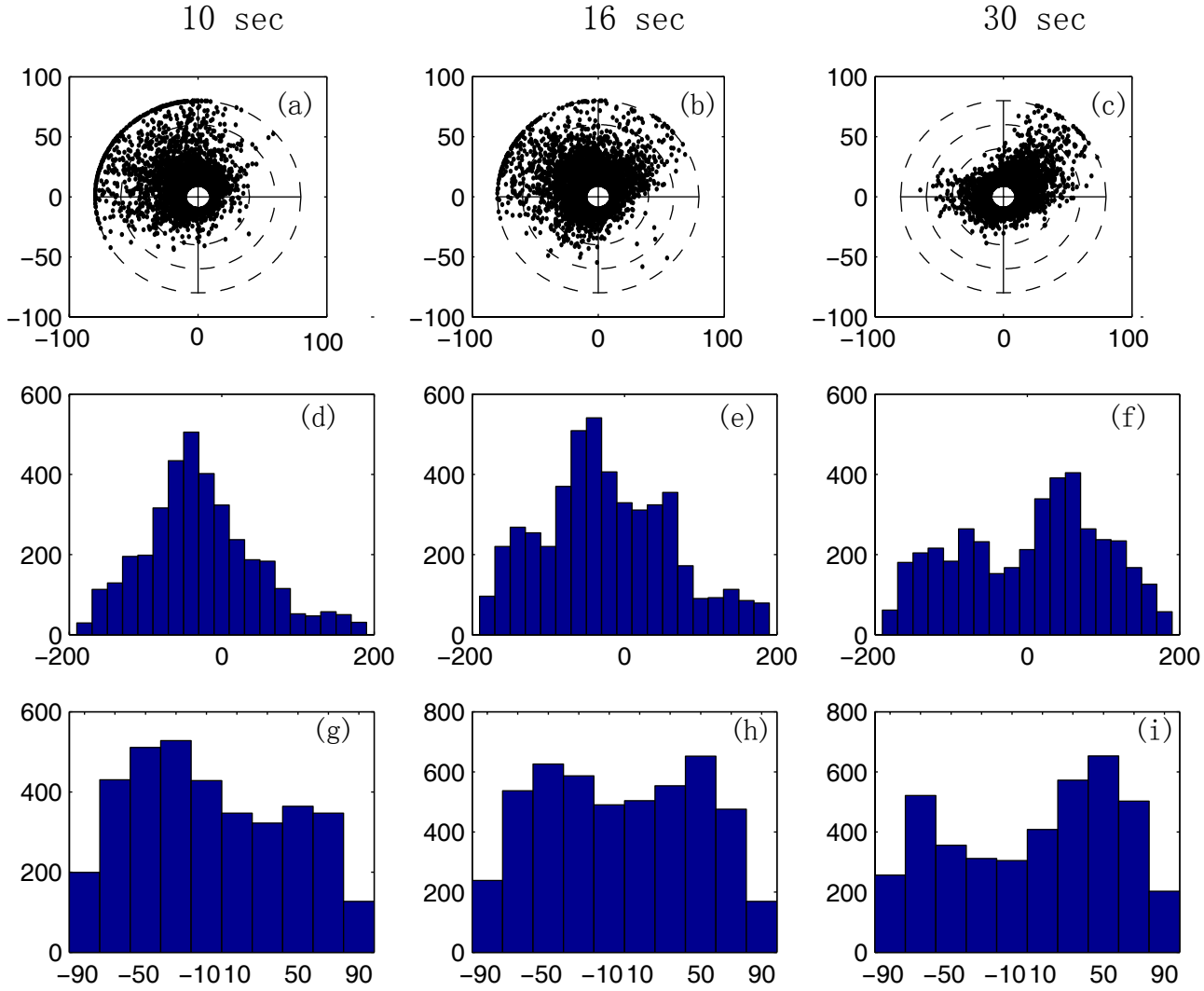
10 sec
16 sec
30 sec
(a)
(b)
(c)
(d)
(e)
(f)
(g)
(h)
(i)

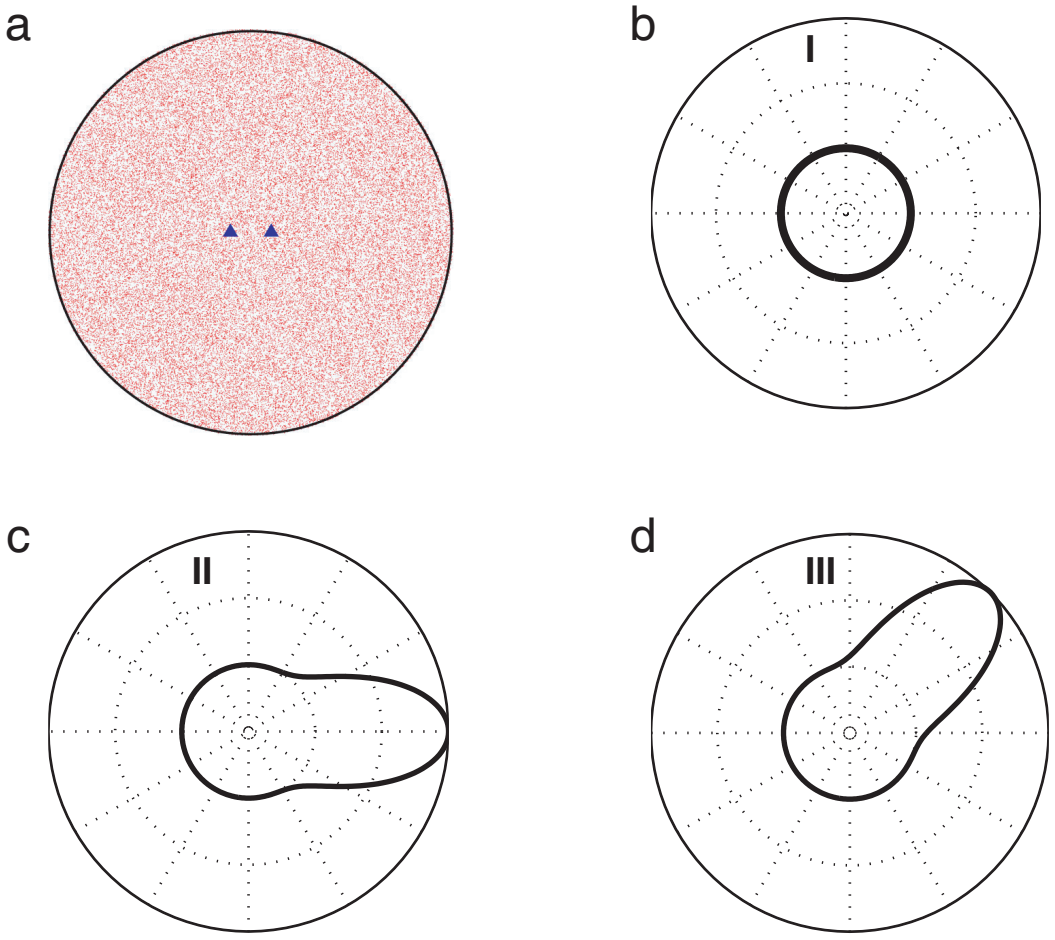
a
b
I
c
II
d
III

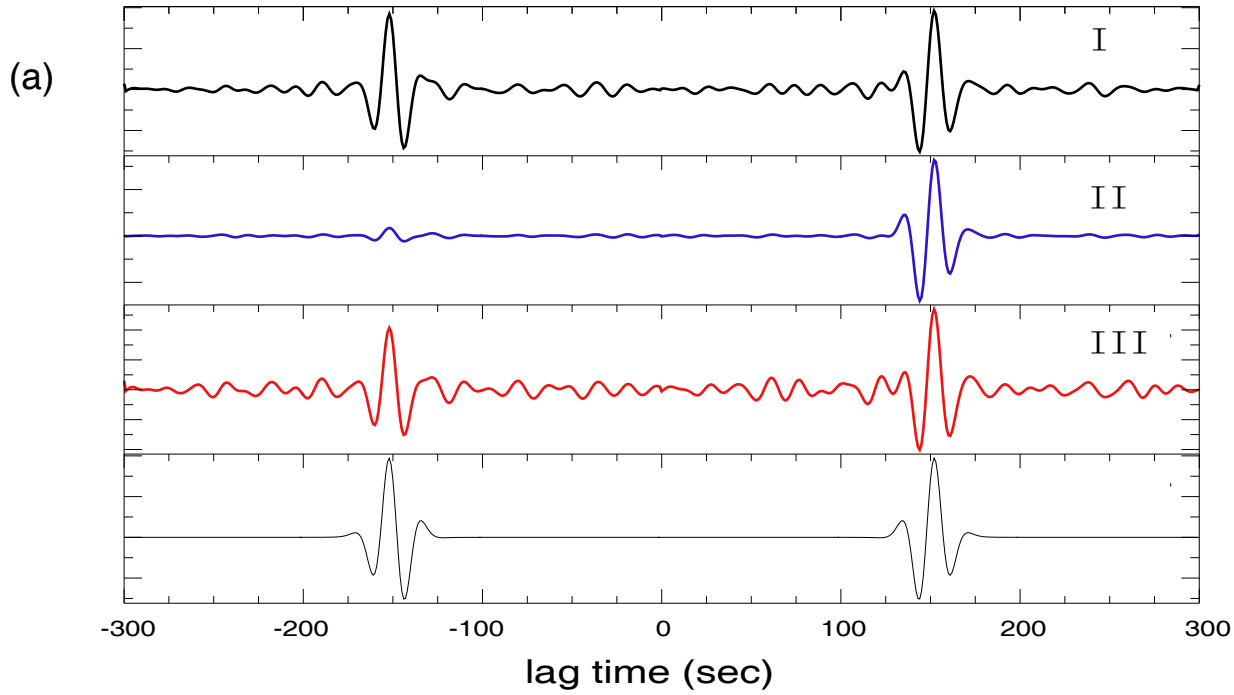
(a)
I
II
III
-300
-200
-100
0
100
200
300
lag time (sec)

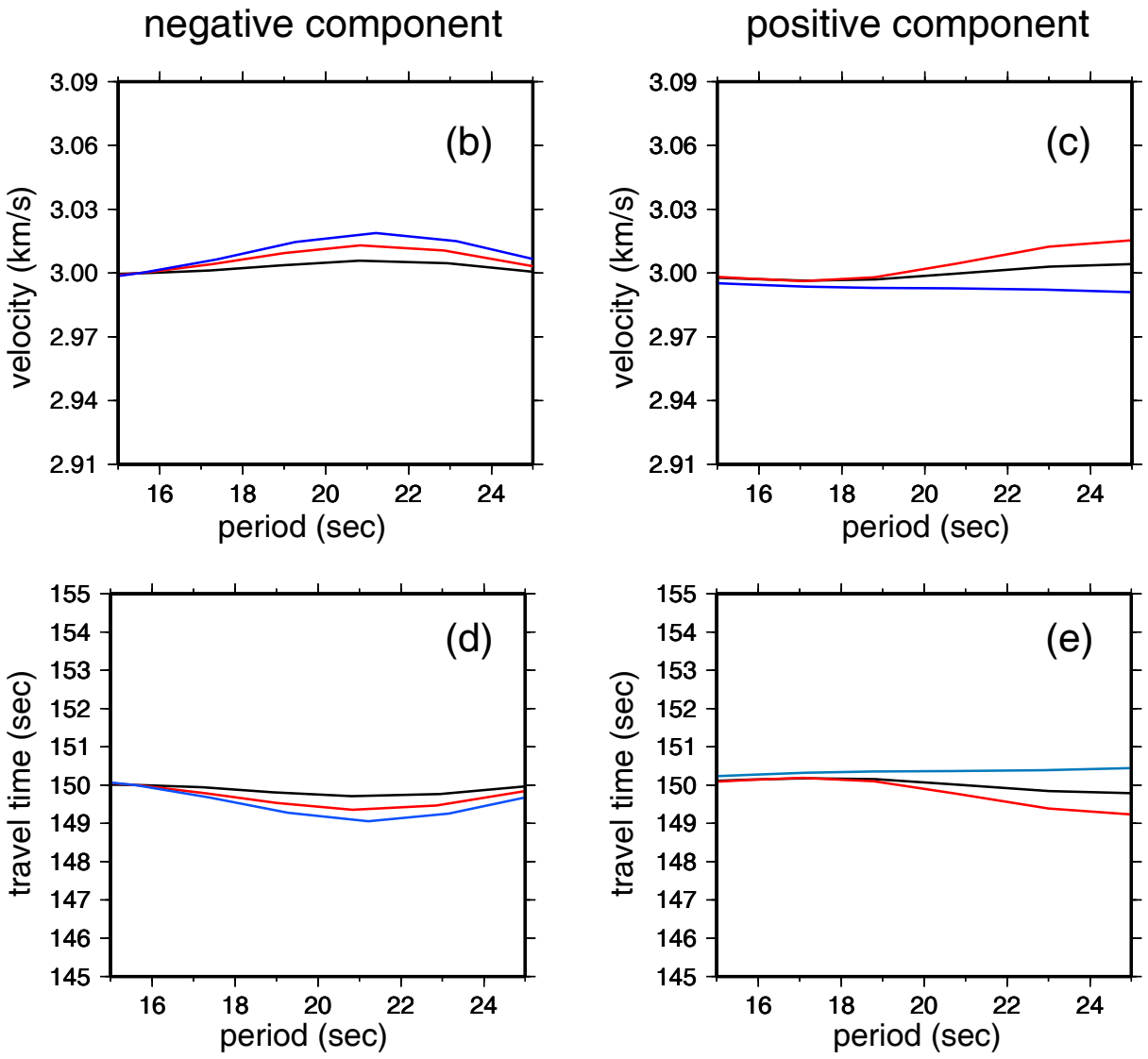
negative component
positive component
(b)
(c)
(d)
(e)
velocity (km/s)
travel time (sec)
period (sec)
3.09
3.06
3.03
3.00
2.97
2.94
2.91
155
154
153
152
151
150
149
148
147
146
145
16
18
20
22
24